

Analysis of KUCA measurements by the reactivity monitoring MATA method

*Original*

Analysis of KUCA measurements by the reactivity monitoring MATA method / Dulla, Sandra; Hoh, SIEW SIN; Marana, Gaia; Nervo, Marta; Ravetto, Piero; Pyeon, Cheol Ho. - In: ANNALS OF NUCLEAR ENERGY. - ISSN 0306-4549. - 101:(2017), pp. 397-407. [10.1016/j.anucene.2016.10.019]

*Availability:*

This version is available at: 11583/2663431 since: 2021-04-06T17:51:48Z

*Publisher:*

Elsevier

*Published*

DOI:10.1016/j.anucene.2016.10.019

*Terms of use:*

This article is made available under terms and conditions as specified in the corresponding bibliographic description in the repository

*Publisher copyright*

Elsevier postprint/Author's Accepted Manuscript

© 2017. This manuscript version is made available under the CC-BY-NC-ND 4.0 license  
<http://creativecommons.org/licenses/by-nc-nd/4.0/>. The final authenticated version is available online at:  
<http://dx.doi.org/10.1016/j.anucene.2016.10.019>

(Article begins on next page)

# Analysis of KUCA measurements by the reactivity monitoring $MA\rho$ TA method

Sandra Dulla<sup>a,\*</sup>, Siew Sin Hoh<sup>a</sup>, Gaia Marana<sup>a</sup>, Marta Nervo<sup>a</sup>, Piero Ravetto<sup>a</sup>, Cheol Ho Pyeon<sup>b</sup>

<sup>a</sup>*NEMO Group, Dipartimento Energia, Politecnico di Torino, Torino, Italy*

<sup>b</sup>*Kyoto University, Research Reactor Institute, Osaka, Japan*

---

## Abstract

A recently developed method for the continuous reactivity monitoring in nuclear reactors and in subcritical source-driven systems is applied for the interpretation of flux measurements carried out in the KUCA facility. The scope of the work is to validate the method using real experimental data. The method is based on general mathematical properties of the differential equations constituting the point kinetic model. Several pulsed experiments performed in different system configurations and using different source target materials are analysed. The results are compared with the classic area ratio method. A good agreement is obtained when the space-energy transient following the source shut-down dies out and when the system sets on a point-like evolution. The results prove the suitability of the proposed method for application to the reactivity monitoring of source-driven systems.

**Keywords:** reactivity monitoring, accelerator-driven systems, KUCA, point kinetics, measurement, neutron pulsed experiments

---

## 1. Introduction

Reactivity monitoring is an important issue in all nuclear multiplying systems. It is of special relevance when dealing with subcritical source-driven systems, since it is extremely important to have immediately information on any change of reactivity that may initiate a potentially dangerous transient. Several methods are available for the

---

\*Corresponding author, sandra.dulla@polito.it

measurement of the reactivity in subcritical systems (Bell and Glasstone, 1970). Many of them refer to pulsed source experiments. For instance, the area ratio method is quite effective and has gained a wide popularity over the years (Sjöstrand, 1956). Of course, these methods cannot provide the information continuously during the operation of the system.

A method for the continuous monitoring of reactivity in source-driven systems is the so-called current-to-flux method (Cao et al., 2013). In recent times a new method named MA $\rho$ TA (Monitoring Algorithm for Reactivity Transient Analysis) has been proposed. The method can be used for systems that normally operate in a critical condition (Dulla et al., 2014a) as well as for subcritical systems sustained by an external source (Dulla et al., 2016). The method has been tested with computationally simulated transients in various configurations, providing promising results. Also tests using literature data (Dulla et al., 2015b) and pulsed experiment measurements (Dulla et al., 2014b) have allowed to draw encouraging conclusions on the capability of the method to interpret real experimental data, even in the presence of non-linear feed-back effects. The basics of the method are shortly outlined in a following section.

The KUCA facility at the Kyoto University constitutes an important undertaking for the current development of accelerator-driven technology. A brief description of the system is given in Section 2. Experiments carried out in KUCA in pulsed source mode provide a unique opportunity to analyse flux measurements by the MA $\rho$ TA method and to validate its performance.

The work presented in this paper has been performed in the frame of the IAEA Coordinated Research Project on Accelerator Driven Systems (ADS) - Application and use of low-enriched uranium. The results illustrated allow to study the applicability of the MA $\rho$ TA method to reactivity monitoring for subcritical system operation.

## **2. Description of the KUCA reactor**

The Kyoto University Critical Assembly (KUCA) (Pyeon et al., 2007, 2015) is a multi-core-type critical assembly developed by the Kyoto University Research Institute (KURRI) (Shiroya et al., 2000, 2002), Japan. It consists of two solid-moderated cores

(A- and B-cores) and one light-water-moderated core (C-core). The A-core is designed to be combined with external neutron sources. Two different sources are available: 14 MeV pulsed neutrons may be generated by D-T (deuterium-tritium) reactions and spallation neutrons can be injected separately into the subcritical system by 100 MeV protons generated from the FFAG (Fixed-Field Alternating Gradient) accelerator.

Currently, in the framework of the activities of the IAEA Coordinated Research Project on Accelerator Driven Systems (ADS) - Application and use of low-enriched uranium, the A-core in source-driven subcritical configuration is used. The experimental campaign is based on pulsed neutron source experiments.

### *2.1. Experimental setting*

The reactor cross view is presented in Fig. 1. The fuel assembly is constituted by highly-enriched uranium with polyethylene reflector layers and their dimensions are specified in Figs. 2 and 3.

Figures 4 through 6 focus on the core configurations used for the experiments whose results are analyzed in this work. They differ in the number of fuel assemblies (25 elements in Cases I, II, III and 21 elements in Cases IV and V) and in the number of control and safety rods inserted into the system. Fully inserted and fully withdrawn rod positions are indicated in the pictures.

The material used for the core assembly is in the form of rectangular prisms, 50.8 mm square with thickness ranging between 1.6 mm and 50.8 mm. The active height of the core is approximately 400 mm. The upper and lower parts of the fuel region are made of reflector layers more than 500 mm long, as shown in Fig. 2.

Spallation neutrons are generated by a 100 MeV proton beam from the FFAG accelerator injected into the system to impinge on different heavy metal targets (i.e., Pb-Bi, W-Be, W). The main features of the accelerator are: 1 nA beam intensity, 20 Hz frequency, 100 ns pulse width, 40 mm diameter spot size at the target and  $1.0 \times 10^8 \text{ s}^{-1}$  neutron yield.

As shown in Fig. 1, the neutron flux monitoring is obtained with three detectors (DET1, DET2 and DET3). DET1 and DET2, located at the axial central positions of the reactor in the reflector region, are  $\text{BF}_3$  detectors and they are 300 mm long and 12.7

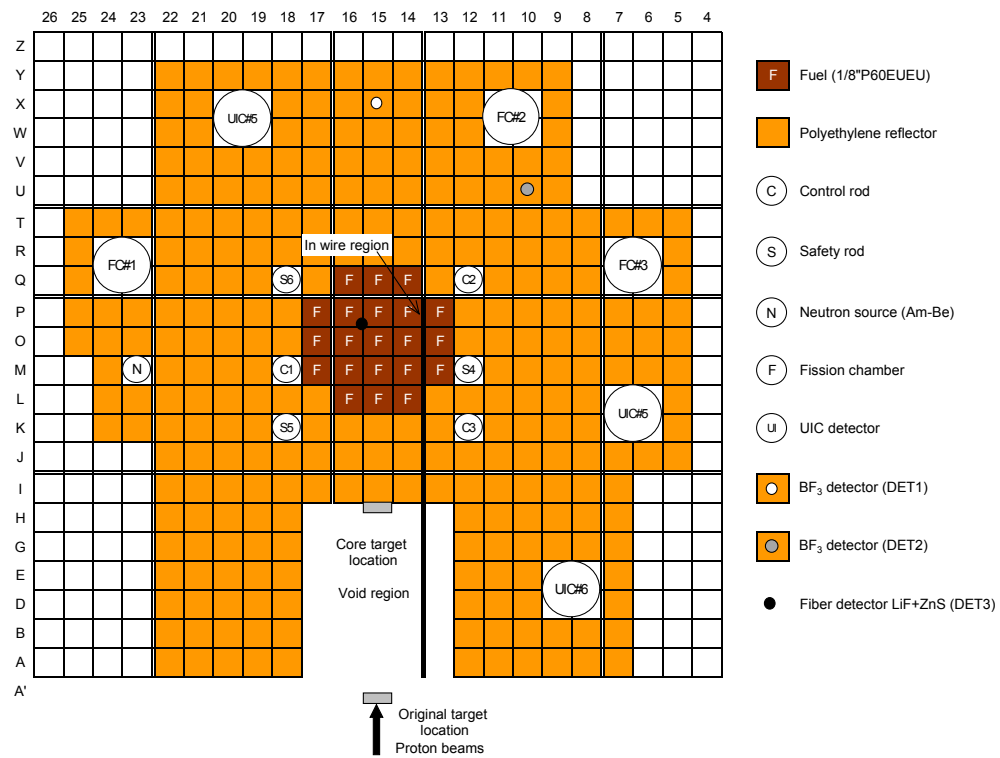


Figure 1: KUCA A-core general configuration.

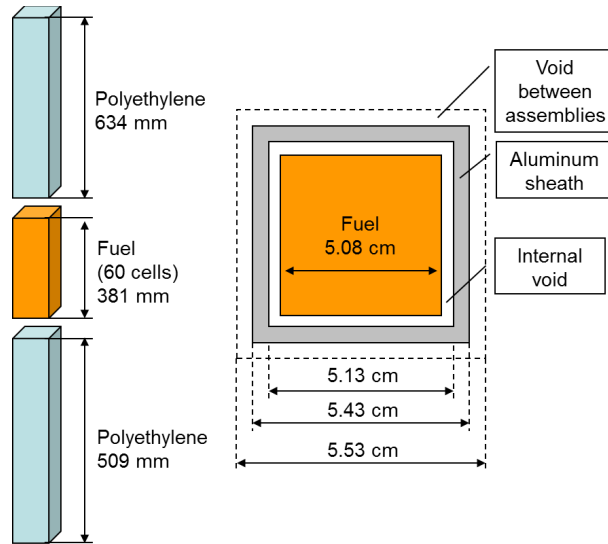


Figure 2: Fuel assembly in KUCA.

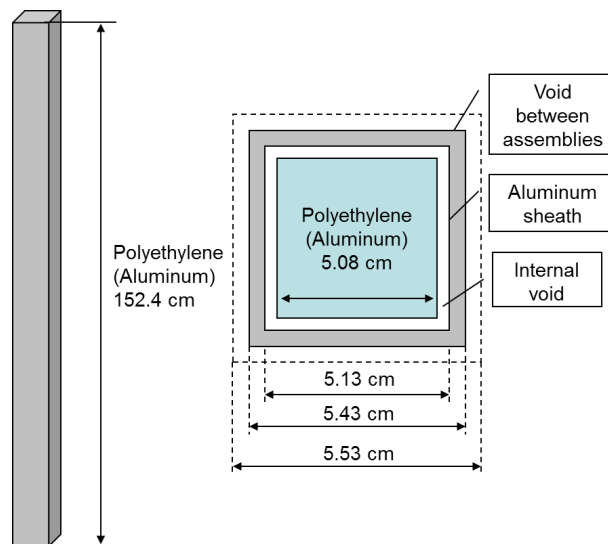


Figure 3: Reflector assembly in KUCA.

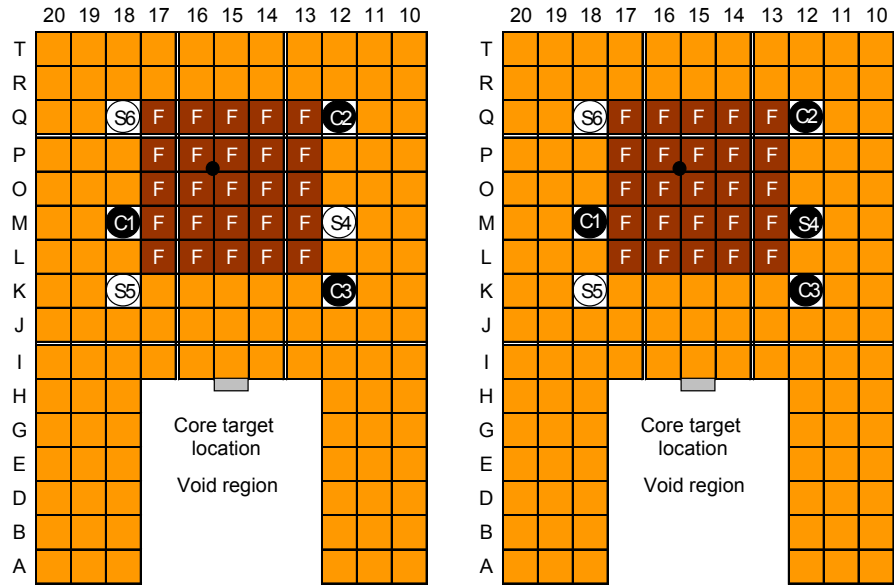


Figure 4: System configurations: Case I (on the left) and Case II (on the right). Inserted and extracted control (C) and safety (S) rods are indicated in black and white, respectively.

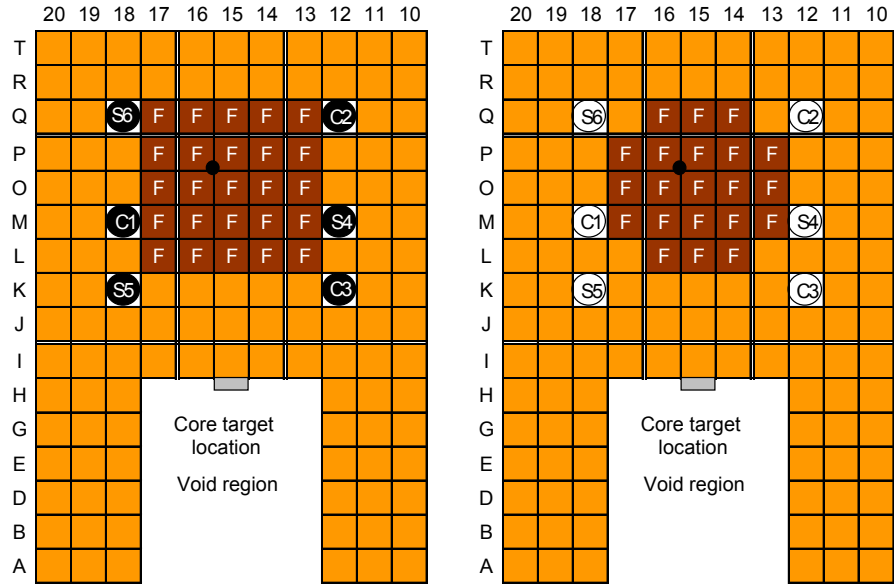


Figure 5: System configurations: Case III (on the left) and Case IV (on the right). Inserted and extracted control (C) and safety (S) rods are indicated in black and white, respectively.

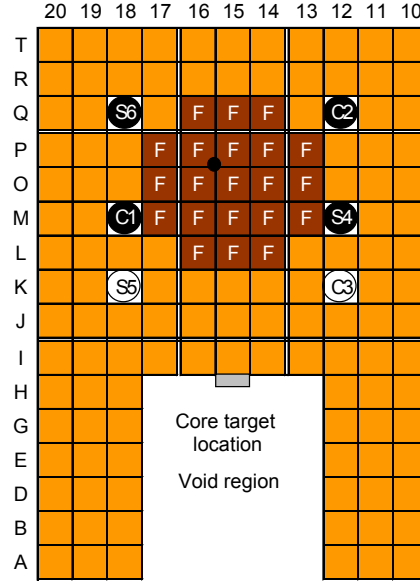


Figure 6: System configuration: Case V. Inserted and extracted control (C) and safety (S) rods are indicated in black and white, respectively.

mm and 25.4 mm diameters respectively. DET3 is an optical fiber detector (LiF+ZnS) placed in the fuel region.

### 3. The MA $\rho$ TA method for the analysis of flux measurements

The MA $\rho$ TA method for reactivity monitoring in nuclear reactors is based on an algorithm derived from the point kinetic model (Akcasu et al., 1971). Therefore, the accuracy of its prediction may be affected by spatial and spectral effects. This problem has already been analysed in previous works (Dulla et al., 2014a) but methods to overcome any drawbacks need further investigation (Dulla et al., 2015a).

From general properties of the differential system of equations constituting the point model it is possible to relate the fundamental time constant to the instantaneous state of the system, i.e. the flux amplitude and the effective delayed neutron concentrations. From the time constant the reactivity can be reconstructed through the inhour relationship. Therefore, the algorithm is a typically inverse technique applied to the



point kinetic system of first-order differential equations.

It can be shown (Dulla et al., 2016) that the fundamental time constant  $\omega$  of the point evolution satisfies the following relationship connecting the flux amplitude  $P(t)$  and the  $M$  effective delayed neutron concentrations  $C_i(t)$ :

$$\dot{P}(t) - \omega_1 P(t) + S_0 + \sum_{i=1}^M \frac{\lambda_i}{\omega_1 + \lambda_i} [\dot{C}_i(t) - \omega_1 C_i(t)] = 0. \quad (1)$$

The value of the effective source  $S_0$  is related to the initial amplitude  $P_0$ , as:

$$P_0 = -\frac{S_0 \Lambda}{\rho_0}. \quad (2)$$

In the case of the absence of the external source, the instantaneous relationship takes the form (Dulla et al., 2014a):

$$\dot{P}(t) - \omega_1 P(t) + \sum_{i=1}^M \frac{\lambda_i}{\omega_1 + \lambda_i} [\dot{C}_i(t) - \omega_1 C_i(t)] = 0. \quad (3)$$

Once the time constant is known, the reactivity is retrieved by the inhour equation:

$$\rho = \omega \Lambda + \sum_{i=1}^M \frac{\beta_i \omega}{\omega + \lambda_i}. \quad (4)$$

In the formulae above the values of the integral reactor parameters  $\Lambda$  (effective mean prompt generation time) and  $\beta_i$  for  $i = 1, 2, \dots, M$  (effective delayed neutron fractions) are supposed to be known from independent measurements (Baeten et al., 2001; Kuramoto et al., 2007) or from numerical simulations. This aspect is rather delicate, since the accuracy of the reactivity prediction obviously depends on such values. In particular, the value of the total effective delayed neutron fraction plays a very important role, since it establishes the unit of measure for the reactivity itself. For instance, the area ratio method yields the reactivity measured in units of the effective delayed neutron fraction. The amplitude of the system  $P$  is the object of the measurement and it is obtained as the flux signal. It is assumed that the flux is measured on a discrete set of time instants (flux sample), while the derivatives are estimated by a proper numerical derivation algorithm applied to the sample of the values of the fluxes.

The information on the effective delayed neutron concentrations can be reconstructed by a time integration of the point model:

$$C_i(t) = C_i(0)e^{-\lambda_i t} + \frac{\beta_i}{\Lambda} \int_0^t P(t')e^{-\lambda_i(t-t')} dt', \quad (5)$$

where the integral can be evaluated by a numerical quadrature formula. The initial condition for the effective concentrations depends on the state of the system at the time the measurement is initiated. If the system is in equilibrium, one can easily state that:

$$C_i(0) = -\frac{S_0\beta_i}{\lambda_i\rho_0}. \quad (6)$$

Otherwise, if considering a sequence of neutron pulses as in the cases analyzed in the following, an equilibrium is reached when the concentration at the end of the neutron cycle of duration  $T$  is equal its initial value, i.e.:

$$C_i(0) = \frac{\frac{\beta_i}{\Lambda} \int_0^T P(t') e^{-\lambda_i(T-t')} dt'}{1 - e^{-\lambda_i T}}. \quad (7)$$

The use of the instantaneous power/flux signals and the numerical estimation of the derivatives appearing in Eq. (1) is affected by the presence of the statistical noise associated to the experimental measurements. In particular, previous analyses have shown that the evaluation of the time derivative of the power is strongly affected by noise, as it is obtained directly from the experimental data (Dulla et al., 2014a, 2016). Instead, the derivative of the precursor concentrations is less problematic, since such concentrations are obtained by an integration process, Eq. (5), that has a beneficial effect on the statistical dispersion. Therefore, filtering techniques are of foremost importance to smooth the amplitude behaviour and to improve the estimation of  $\dot{P}$  (Dulla et al., 2016), in order to make the application of the method viable for real applications. In particular, the amplitude signals obtained experimentally are pre-processed adopting a moving mean filter (Savitzky and Golay, 1964), in order to reduce the statistical oscillations of the values entering formula in Eq. (3). The derivative of the amplitude is then evaluated adopting a specific algorithm developed for the calculation of derivative of noisy data (Chartrand, 2011). The precursor concentrations are evaluated by performing numerically the integral in Eq. (5) with the smoothed amplitude data, while their derivatives are obtained applying a standard backward Euler discretization.

The present work deals with the analysis of pulsed experiments in KUCA. The interpretation algorithm is applied in the source-free mode, Eq. (3), considering the flux measurements only after the shutdown of the source and the results obtained are com-

pared to the values obtained by the application of the area ratio method as performed by the staff at KURRI.

The evaluation of the statistical uncertainty related to the reactivity estimation with MA $\rho$ TA can be performed as follows. We start considering Eq. (3) evaluated at a certain time instant  $t_j$ , where the period  $T$  of the pulsed source has been discretized into  $N$  equally spaced time points, coherently with the available experimental data:

$$H(\omega_j, P_1, P_2, \dots, P_j, \dots, P_N) = \dot{P}(t_j) - \omega_j P_j + \sum_{i=1}^M \frac{\lambda_i}{\omega_j + \lambda_i} [\dot{C}_i(t_j) - \omega_j C_i(t_j)] = 0. \quad (8)$$

The time constant  $\omega$  has the subscript  $j$  to indicate that it is the value of  $\omega$  obtained applying MA $\rho$ TA at time  $t_j$ . The time derivatives in Eq. (8) are then evaluated as described above:

$$H(\omega_j, P_1, P_2, \dots, P_j, \dots, P_N) = \dot{P}_j(P_1, P_2, \dots, P_N) - \omega_j P_j + \sum_{i=1}^M \frac{\lambda_i}{\omega_j + \lambda_i} \left[ \frac{C_i(t_j) - C_i(t_{j-1})}{\Delta t} - \omega_j C_i(t_j) \right] = 0. \quad (9)$$

It should be noticed that the use of the algorithm for differentiation of noisy data introduce a dependence of the derivative at time  $t_j$  with respect to all time instants in the period, as they are all fed into the algorithm. A further step can be performed introducing a simple quadrature scheme for the integral term involved in the evaluation of the delayed neutron effective concentrations, see Eq. (5), applied to both the values at time  $t_j$  and  $t_{j-1}$ :

$$\begin{aligned} & H(\omega_j, P_1, P_2, \dots, P_j, \dots, P_N) \\ &= \dot{P}_j(P_1, P_2, \dots, P_N) - \omega_j P_j - \sum_{i=1}^M \frac{\lambda_i}{\omega_j + \lambda_i} \left[ \frac{1}{\Delta t} C_i(t_{j-1}) + \left( \omega_j - \frac{1}{\Delta t} \right) C_i(t_j) \right] \\ &= \dot{P}_j(P_1, P_2, \dots, P_N) - \omega_j P_j - \sum_{i=1}^M \frac{\lambda_i}{\omega_j + \lambda_i} \cdot \\ & \quad \left[ \frac{1}{\Delta t} \left( C_i(0) e^{-\lambda_i t_{j-1}} + \frac{\beta_i}{\Lambda} \sum_{m=1}^{j-1} \Delta t P_m e^{-\lambda_i (t_{j-1} - t_m)} \right) \right. \\ & \quad \left. + \left( \omega_j - \frac{1}{\Delta t} \right) \left( C_i(0) e^{-\lambda_i t_j} + \frac{\beta_i}{\Lambda} \sum_{m=1}^j \Delta t P_m e^{-\lambda_i (t_j - t_m)} \right) \right] = 0. \end{aligned} \quad (10)$$

In expression (10) also the initial concentrations  $C_i(0)$  are depending on all amplitudes values, due to the imposed condition in Eq. (7), discretized consistently with the other integrals.

The uncertainty on the value  $\omega_j$  obtained from expression in Eq. (10) can be calculated adopting the standard first-order Taylor expansion of the dependence on  $P$ , leading to the general expression for the variance:

$$\text{var}(\omega_j) = \sum_{\ell=1}^N \left( \frac{\partial \omega_j}{\partial P_\ell} \right)^2 \text{var}(P_\ell) + 2 \sum_{\ell=1}^N \sum_{m=\ell+1}^N \frac{\partial \omega_j}{\partial P_\ell} \frac{\partial \omega_j}{\partial P_m} \text{cov}(P_\ell, P_m). \quad (11)$$

The amplitude signals  $P_j$  are obtained by neutron detector counting rates and are assumed uncorrelated. However, the  $P$  values used in the MA $\rho$ TA algorithm are the ones smoothed by the application of the moving mean filter, thus introducing a correlation among the  $P$  values.

To evaluate  $\text{var}(\omega_j)$  it is then necessary to calculate the derivatives appearing in Eq. (11); this can be done starting from the following expression:

$$\frac{\partial \omega_j}{\partial P_\ell} = - \frac{\partial H_j / \partial P_\ell}{\partial H_j / \partial \omega_j}, \quad (12)$$

where the index  $j$  attached to  $H$  denotes that the time constant  $\omega_j$  is evaluated considering the function  $H$  at the time instant  $t_j$ . The derivatives on the right-hand-side of

Eq. (12) are calculated as follows:

$$\frac{\partial H_j}{\partial P_\ell} = \frac{\partial \dot{P}_j}{\partial P_\ell} - \omega_j + \sum_{i=1}^M \frac{\lambda_i}{\omega_j + \lambda_i} \left[ \frac{\partial C_i(0)}{\partial P_\ell} e^{-\lambda_i t_j} \left( \frac{1}{\Delta t} - \frac{1}{\Delta t} e^{\lambda_i \Delta t} - \omega \right) + \frac{\beta}{\Lambda} (1 - \omega \Delta t) \right]$$

for  $\ell = j$ ,

$$\begin{aligned} \frac{\partial H_j}{\partial P_\ell} = \frac{\partial \dot{P}_j}{\partial P_\ell} + \sum_{i=1}^M \frac{\lambda_i}{\omega_j + \lambda_i} & \left[ \frac{\partial C_i(0)}{\partial P_\ell} e^{-\lambda_i t_j} \left( \frac{1}{\Delta t} - \frac{e^{\lambda_i \Delta t}}{\Delta t} - \omega_j \right) \right. \\ & \left. + \frac{\beta}{\Lambda} e^{-\lambda_i (t_j - t_\ell)} (1 - e^{\lambda_i \Delta t} - \omega_j \Delta t) \right] \end{aligned} \quad \text{for } \ell < j,$$

$$\frac{\partial H_j}{\partial P_\ell} = \frac{\partial \dot{P}_j}{\partial P_\ell} + \sum_{i=1}^M \frac{\lambda_i}{\omega_j + \lambda_i} \left[ \frac{\partial C_i(0)}{\partial P_\ell} e^{-\lambda_i t_j} \left( \frac{1}{\Delta t} - \frac{e^{\lambda_i \Delta t}}{\Delta t} - \omega_j \right) \right] \quad \text{for } \ell > j,$$

$$\begin{aligned} \frac{\partial H_j}{\partial \omega_j} = -P_j - \sum_{i=1}^M \frac{\lambda_i}{(\omega_j + \lambda_i)^2} & \left[ C_i(0) e^{-\lambda_i t_j} \left( \frac{1}{\Delta t} - \frac{e^{\lambda_i \Delta t}}{\Delta t} - \lambda_i \right) \right. \\ & \left. + \frac{\beta}{\Lambda} (1 - \lambda_i \Delta t) \sum_{m=1}^j P_m e^{-\lambda_i (t_j - t_m)} - \frac{\beta}{\Lambda} \sum_{m=1}^{j-1} P_m e^{-\lambda_i (t_j - t_m)} \right]. \end{aligned} \quad (13)$$

In the above formulae the derivatives of  $C_i(0)$  and  $\dot{P}$  with respect to the power values are needed. While the first can be calculated explicitly from relation in Eq. (7):

$$\frac{\partial C_i(0)}{\partial P_\ell} = \frac{\beta}{\Lambda} \Delta t \frac{e^{-\lambda_i (T - t_\ell)}}{1 - e^{-\lambda_i T}}, \quad (14)$$

the derivative for  $\dot{P}$  has been evaluated numerically with a finite difference approximation

$$\frac{\partial \dot{P}_j}{\partial P_\ell} \approx \frac{\dot{P}_j(P_1, \dots, P_\ell, \dots, P_N) - \dot{P}_j(P_1, \dots, P_\ell - h, \dots, P_N)}{h}, \quad (15)$$

where the value  $h$  has been taken in the same order as the uncertainty on the  $P$  values, and the algorithm for the derivative of noisy data has been applied twice for each derivative calculation.

The uncertainty on the time constant  $\omega_j$  is then used to evaluate the corresponding variance of the instantaneous reactivity value, obtained through the inhour equation (4):

$$\text{var}(\rho_j) = \left( \frac{\partial \rho_j}{\partial \omega_j} \right)^2 \text{var}(\omega_j) = \left( \Lambda + \sum_{i=1}^M \frac{\beta_i \lambda_i}{(\omega_j + \lambda_i)^2} \right)^2 \text{var}(\omega_j). \quad (16)$$

For the analysis of pulsed experiments, starting from this set of  $\rho_j$  values, the best estimate for  $\rho$  may be assumed to be the average on a sample including  $N_{av}$  values obtained during the time interval under analysis following the source shut-down, to be evaluated together with its statistical error:

$$\begin{aligned}\bar{\rho} &= \frac{1}{N_{av}} \sum_{j=(N-N_{av})+1}^N \rho_j, \\ \text{var}(\bar{\rho}) &= \frac{1}{N_{av}^2} \sum_{j=(N-N_{av})+1}^N \text{var}(\rho_j) + \frac{2}{N_{av}^2} \sum_{j=(N-N_{av})+1}^N \sum_{k=j+1}^N \text{cov}(\rho_j, \rho_k).\end{aligned}\tag{17}$$

The covariance among the  $\rho$  values can be expressed as:

$$\begin{aligned}\text{cov}(\rho_j, \rho_k) &= \frac{\partial \rho_j}{\partial \omega_j} \frac{\partial \rho_k}{\partial \omega_k} \text{cov}(\omega_j, \omega_k) \\ \text{cov}(\omega_j, \omega_k) &= \sum_{n=1}^N \frac{\partial \omega_j}{\partial P_n} \frac{\partial \omega_k}{\partial P_n} \text{var}(P_n) + \sum_{n=1}^N \sum_{\substack{m=1 \\ m \neq n}}^N \frac{\partial \omega_j}{\partial P_n} \frac{\partial \omega_k}{\partial P_m} \text{cov}(P_n, P_m).\end{aligned}\tag{18}$$

A parametric analysis can be performed on the most appropriate number  $N_{av}$  of values to be considered in the average, starting from the end of the period  $T$  and proceeding backwards (e.g. averaging the last  $N_{av}$  values of reactivity obtained), since one can assume that towards the end of the pulse response considered the space-energy effects may be reasonably considered to have died out.

#### 4. Results and discussion

The MA $\rho$ TA algorithm is now applied to some pulsed experiments performed at KUCA, analysing the flux signals recorded after the shut-down of the external source. The data for the delayed neutron families used, obtained from simulations by MCNP-6 with ENDF/B-VII.0 data library, are reported in Table 1 (Pyeon, 2014). The prompt neutron generation time  $\Lambda$  is 30.5  $\mu\text{s}$ . The same integral data are assumed for all experimental configurations considered, although differences may actually exist. For instance the use of different targets may cause a difference in the source neutron energy distribution, thus producing a difference in the spectrum that can affect the system integral parameters.

Table 1: Values of effective delayed neutron fractions  $\beta_i$  and decay constants  $\lambda_i$  for the six-family delayed neutron families adopted for the KUCA reactor evaluation.

$i$	$\lambda_i$ [s <sup>-1</sup> ]	$\beta_i$ [pcm]
1	0.01249	24
2	0.03182	134
3	0.10938	130
4	0.31700	371
5	1.35393	110
6	8.63759	38
		$\beta = 807$ pcm

Figures from 7 to 9 show the detector signals for all the reactor configurations with the Pb-Bi target. The flux signals are taken with a time interval of 10  $\mu$ s. It is possible to observe that all these flux measurements appear to show a point-like behavior (the trend of the curves are the same for all three detectors) and they seem not to be heavily affected by statistical uncertainties. Such features are promising for the application of inverse algorithms.

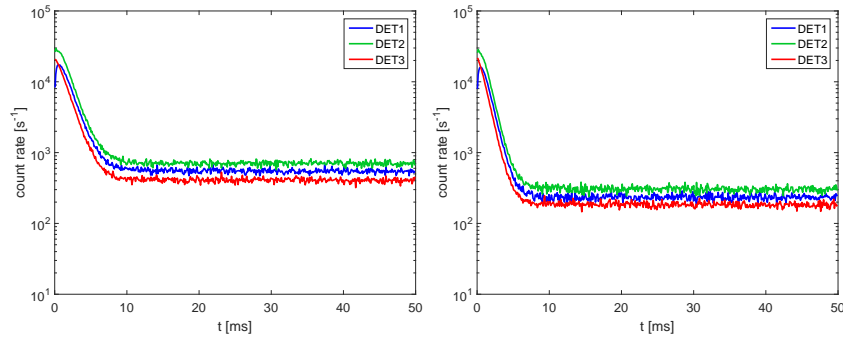


Figure 7: Detector signals for Case I (left) and for Case II (right) with Pb-Bi target.

The introduction of the moving mean filter to smooth the signals analysed is also investigated (Savitzky and Golay, 1964). This procedure is adopted with sets of 5 points

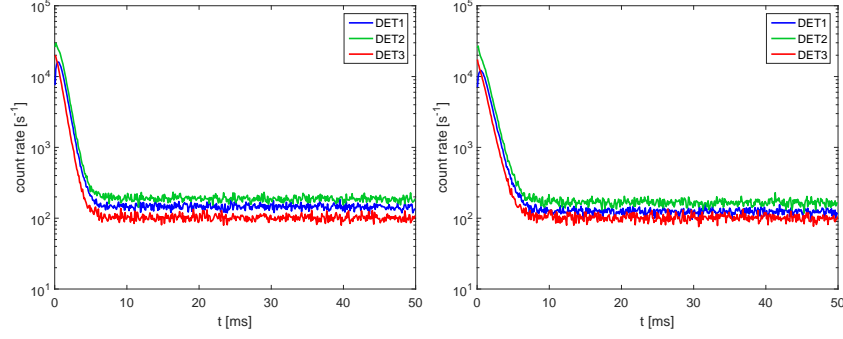


Figure 8: Detector signals for Case III (left) and for Case IV (right) with Pb-Bi target.

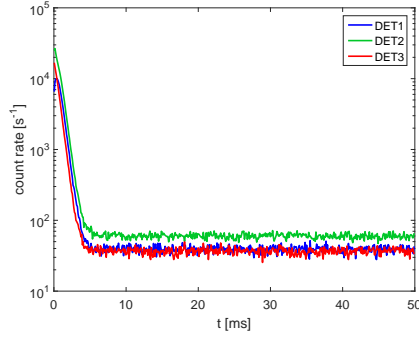


Figure 9: Detector signals for Case V with Pb-Bi target.

each. The effect of the smoothing procedure can be observed in Figs. 10 and 11. Here, as an example, two different detectors are considered: the original and the filtered flux measurements are shown and the corresponding reactivity estimations at each time instant are compared. These results demonstrate the effectiveness of the filtering process, even in the case of the noisy signal characterizing Case V. In the following analysis all the detector signals are dealt with the moving mean filter.

The instantaneous reactivity is reported in Figs. 12 through 14 for some selected detectors and configurations. The instantaneous value of the reactivity in the first portion of the period is strongly affected by the presence of the source, generating a flux evolution that cannot be accurately described by the point model. Afterwards, the values stabilize, although oscillations appear due to the noise of the original signal. The



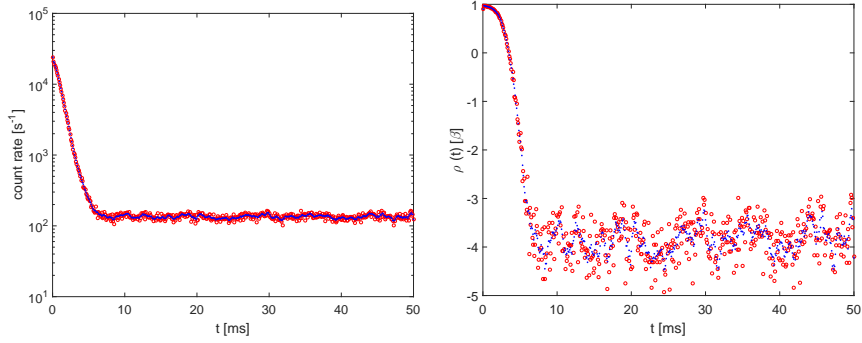


Figure 10: Signal (left) and reactivity prediction (right) for DET3 of Case II with W target. Blue dots denote the filtered signal and the corresponding reactivity prediction.

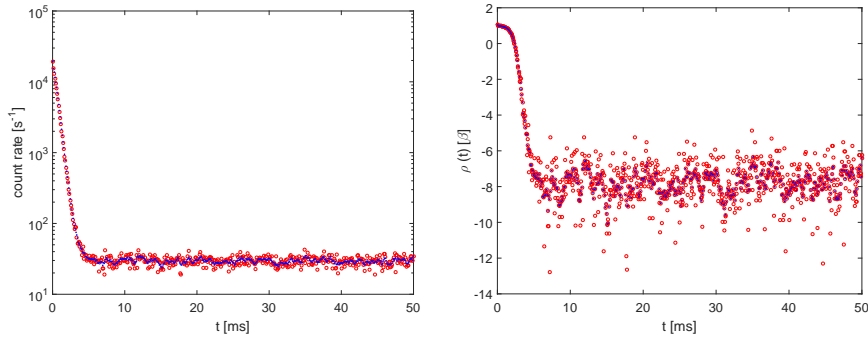


Figure 11: Signal (left) and reactivity (right) for DET3 of Case V with W target. Blue dots denote the filtered signal and the corresponding reactivity prediction.

off-line reactivity evaluations using the area ratio method are also reported on these graphs. After reaching the point-like behavior, a good agreement between the two approaches is appearing, although it seems that the area ratio method yields a value slightly higher than the time-averaged value obtained by  $MA\rho TA$  (see also Tables 2-4). The difference observed can be associated to the value of the effective delayed neutron fraction that is adopted in  $MA\rho TA$  (see Table 1) to obtain the reactivity values and then convert them into dollars, in order to compare to the area ratio method results given by KURRI. The value of  $\beta$  adopted is not influencing the area ratio method when results are given in dollars, while it is affecting the  $MA\rho TA$  results, as was shown in previous

studies through a sensitivity analysis (Dulla et al., 2014a). The small bias observed between  $MA\rho TA$  and the area ratio method can thus be associated to the uncertainty on the  $\beta$  value adopted, since its evaluation/measurement in nuclear systems always constitutes a delicate issue.

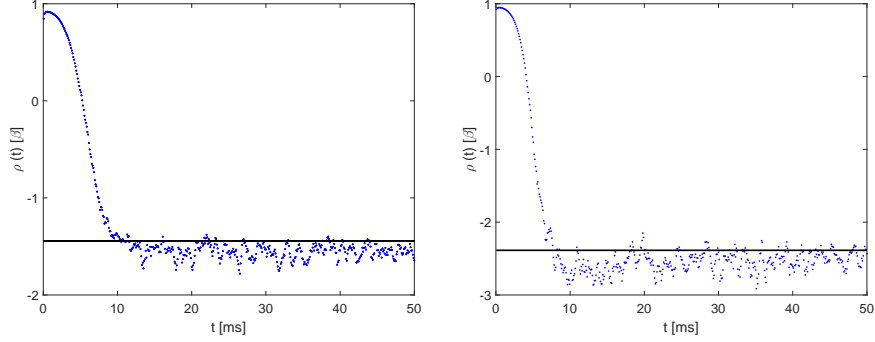


Figure 12: Evaluation of  $\rho(t)$  (blue dot) by  $MA\rho TA$  and by the area ratio method (black line) for DET1 in Case I (left) and Case II (right) with the Pb-Bi target.

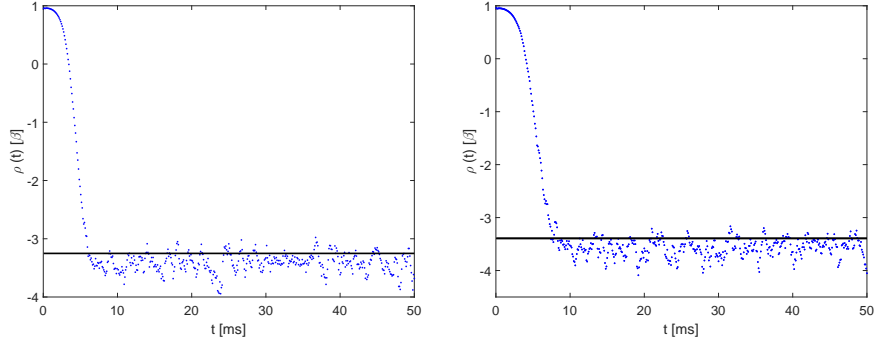


Figure 13: Evaluation of  $\rho(t)$  (blue dot) by  $MA\rho TA$  and by the area ratio method (black line) for DET1 in Case III (left) and Case IV (right) with the Pb-Bi target.

The time-averaged reactivity  $\bar{\rho}$  with its associated uncertainty is also evaluated following the procedure described above. The parametric analysis on the sample size  $N_{av}$  is performed and the results are sketched in Figs. 15 through 17. Increasing the dimension of the sample obviously reduces the uncertainty  $\sigma_{\bar{\rho}}$ . However, when the sample is so large to include the first portion of the period, poor results are obtained because of

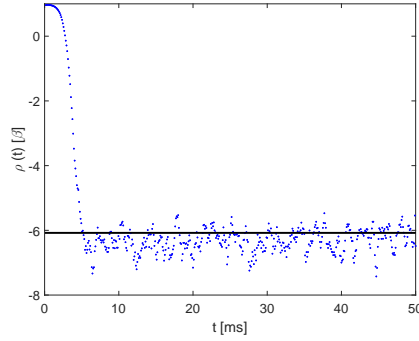


Figure 14: Evaluation of  $\rho(t)$  (blue dot) by  $\text{MA}\rho\text{TA}$  and by the area ratio method (black line) for DET1 in Case V with the Pb-Bi target.

the non-point-like behavior.

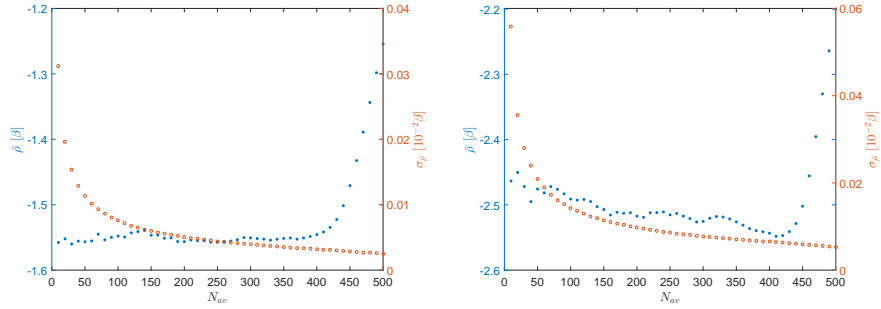


Figure 15: Evaluation of  $\bar{\rho}$  and  $\sigma_{\bar{\rho}}$  with different sample dimensions ( $N_{av}$ ) for DET1 in Case I (left) and Case II (right) with the Pb-Bi target. Blue dots:  $\bar{\rho}$ , open red circles:  $\sigma_{\bar{\rho}}$ .

The values of  $\bar{\rho}$  appear to stabilize for all the cases considered. Tables 2, 3 and 4 summarize the results  $\bar{\rho}$  and  $\sigma_{\bar{\rho}}$ , assuming a sample with  $N_{av} = 300$ . The discrepancy with respect to the evaluations obtained by the area ratio method is also reported, showing a good consistency of the results. The negative bias, as already observed, is due to the value of the effective delayed neutron fraction adopted.

The reactivity estimations obtained for Cases I, II, III and IV are satisfactory. The values of  $\bar{\rho}$  are in good agreement with the ones obtained by the area ratio method and the associated values of  $\sigma_{\bar{\rho}}$  are acceptable. The Case V, the most subcritical core con-

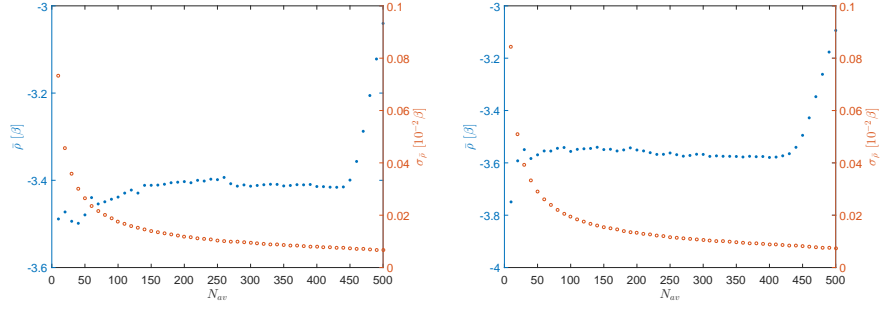


Figure 16: Evaluation of  $\bar{\rho}$  and  $\sigma_{\bar{\rho}}$  with different sample dimensions ( $N_{av}$ ) for DET1 in Case III (left) and Case IV (right) with the Pb-Bi target. Blue dots:  $\bar{\rho}$ , open red circles:  $\sigma_{\bar{\rho}}$ .

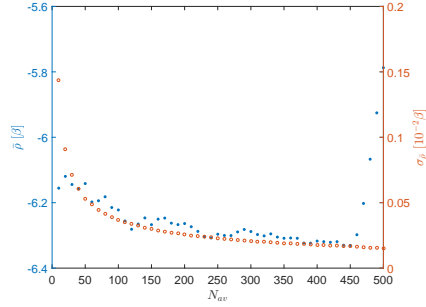


Figure 17: Evaluation of  $\bar{\rho}$  and  $\sigma_{\bar{\rho}}$  with different sample dimensions ( $N_{av}$ ) for DET1 in Case V with the Pb-Bi target. Blue dots:  $\bar{\rho}$ , open red circles:  $\sigma_{\bar{\rho}}$ .

figuration, is characterized by larger, although still acceptable, values of  $\sigma_{\bar{\rho}}$ . Such outcome is due to the more relevant noise affecting the experimental signals. In all the experiments small spatial effects are experienced: this can be physically explained by the deep subcriticality of the system, which causes a more point-like response (Bosio et al., 2001; Eriksson et al., 2005).

The analysis of the experimental data from the KUCA facility demonstrate the capability of the method proposed to attain adequate reactivity predictions in several different reactor core configurations and sources. Furthermore the comparison with the estimations obtained using the area ratio method confirms the consistency of the technique proposed.

Table 2: Average values of the reactivity  $\bar{\rho}$  and corresponding uncertainty  $\sigma = \sqrt{\text{var}}$  evaluated with a sample size  $N_{av} = 300$ , for all the reactor configurations with Pb-Bi target. The difference with respect to the area ratio method (AM) results is also reported.

	Detector	$\bar{\rho}$ [ $\beta$ ]	$\sigma_{\bar{\rho}}$ [ $10^{-2}\beta$ ]	$\rho_{AM}$ [ $\beta$ ]	$\sigma_{\rho_{AM}}$ [ $10^{-2}\beta$ ]	$\bar{\rho} - \rho_{AM}$ [ $10^{-2}\beta$ ]
Case I	DET1	-1.55	0.5	-1.44	2.2	-10.6
	DET2	-1.83	0.6	-1.72	2.5	-11.2
	DET3	-1.82	0.6	-1.72	2.5	-10.0
Case II	DET1	-2.53	1.0	-2.39	3.6	-13.9
	DET2	-3.07	1.1	-2.92	4.3	-14.8
	DET3	-2.91	0.9	-2.79	4.1	-11.5
Case III	DET1	-3.41	1.2	-3.25	4.8	-16.2
	DET2	-4.18	1.5	-4.01	5.9	-16.6
	DET3	-3.80	1.6	-3.69	5.6	-11.1
Case IV	DET1	-3.57	1.3	-3.39	5.1	-17.5
	DET2	-4.27	1.6	-4.09	6.1	-17.5
	DET3	-3.75	1.5	-3.62	5.5	-12.5
Case V	DET1	-6.29	2.6	-6.08	9.5	-21.3
	DET2	-8.08	2.6	-7.88	11.4	-20.0
	DET3	-6.16	2.6	-6.09	9.2	-7.5

## 5. Conclusions

In this work the inverse technique known as MA $\rho$ TA is tested through the interpretation of flux measurements carried out on the KUCA reactor. The comparison of the results with the ones obtained by the area ratio method shows that the technique can yield adequate prediction of the reactivity. It can therefore be proposed as an on-line monitoring technique in subcritical source-driven systems.

In some applications, especially for systems near criticality or when the response is strongly affected by the presence of the source, spatial and spectral effects may greatly

Table 3: Average values of the reactivity  $\bar{\rho}$  and corresponding uncertainty  $\sigma = \sqrt{\text{var}}$  evaluated with a sample size  $N_{av} = 300$ , for all the reactor configurations with W-Be target. The difference with respect to the area ratio method (AM) results is also reported.

	Detector	$\bar{\rho}$ [ $\beta$ ]	$\sigma_{\bar{\rho}}$ [ $10^{-2}\beta$ ]	$\rho_{AM}$ [ $\beta$ ]	$\sigma_{\rho_{AM}}$ [ $10^{-2}\beta$ ]	$\bar{\rho} - \rho_{AM}$ [ $10^{-2}\beta$ ]
Case I	DET1	-1.52	0.5	-1.42	2.2	-10.3
	DET2	-1.91	0.6	-1.81	2.6	-10.7
	DET3	-1.92	0.5	-1.83	2.6	-9.8
Case II	DET1	-2.46	0.8	-2.33	3.5	-13.0
	DET2	-3.19	1.2	-3.05	4.5	-13.4
	DET3	-2.86	1.1	-2.76	4.1	-10.0
Case III	DET1	-3.25	1.3	-3.10	4.8	-14.5
	DET2	-4.37	1.7	-4.22	6.3	-15.2
	DET3	-3.73	1.7	-3.64	5.6	-8.6
Case IV	DET1	-3.50	1.4	-3.33	5.1	-16.7
	DET2	-4.48	1.8	-4.32	6.4	-16.8
	DET3	-3.71	1.4	-3.61	5.3	-10.8
Case V	DET1	-6.40	3.2	-6.20	10.3	-19.9
	DET2	-8.94	5.0	-8.74	14.1	-20.5
	DET3	-6.13	3.1	-6.11	9.5	-1.9

influence the accuracy of the reactivity predictions by the MA $\rho$ TA technique. Some attempts to mitigate such effects have been preliminarily studied. However, such ideas must be verified in real experiments, such as the ones available from the KUCA facility. This constitutes an effort that is currently going on.

The performance of the prediction algorithm is influenced by the values of the integral parameters that are considered as input to the method. In the present work an effect of the effective delayed neutron fraction has been observed, Also the value of the effective mean prompt generation time can play an important role. Future works must be devoted to further investigations on the computational evaluations and on the

Table 4: Average values of the reactivity  $\bar{\rho}$  and corresponding uncertainty  $\sigma = \sqrt{\text{var}}$  evaluated with a sample size  $N_{av} = 300$ , for all the reactor configurations with W target. The difference with respect to the area ratio method (AM) results is also reported.

	Detector	$\bar{\rho}$ [ $\beta$ ]	$\sigma_{\bar{\rho}}$ [ $10^{-2}\beta$ ]	$\rho_{AM}$ [ $\beta$ ]	$\sigma_{\rho_{AM}}$ [ $10^{-2}\beta$ ]	$\bar{\rho} - \rho_{AM}$ [ $10^{-2}\beta$ ]
Case I	DET1	-1.50	0.2	-1.40	2.1	-9.9
	DET2	-1.83	0.4	-1.73	2.5	-10.4
	DET3	-2.47	0.5	-2.34	3.3	-12.8
Case II	DET1	-2.45	0.6	-2.33	3.3	-12.0
	DET2	-3.05	0.8	-2.93	4.3	-12.5
	DET3	-3.85	1.2	-3.72	5.5	-12.8
Case III	DET1	-3.12	0.9	-2.97	4.3	-14.9
	DET2	-4.07	1.3	-3.91	5.7	-16.0
	DET3	-4.88	2.0	-4.74	7.2	-14.4
Case IV	DET1	-3.50	1.1	-3.32	4.8	-17.3
	DET2	-4.25	1.5	-4.08	5.9	-17.0
	DET3	-4.70	2.0	-4.55	6.8	-15.3
Case V	DET1	-6.33	2.6	-6.13	9.7	-20.4
	DET2	-8.13	4.2	-7.91	12.5	-21.7
	DET3	-7.78	4.2	-7.72	12.3	-6.4

measurements techniques for a more accurate estimation of these parameters, that play a fundamental role in all inverse techniques.

### Acknowledgments

This work is performed within the framework of the IAEA Coordinated Research Project on Accelerator Driven Systems (ADS) - Application and use of low-enriched uranium.

## References

- Akcasu, Z., Lellouche, G., Shotkin, L., 1971. *Mathematical methods in nuclear reactor dynamics*. Academic Press, New York.
- Baeten, P., Paepen, J., van der Meer, K., Ait Abderrahim, H., 2001. Absolute measurement of  $\beta_{eff}$  and  $l$  on weapon-grade MOX fuel at the VENUS critical facility by means of the RAPJA technique. *Annals of Nuclear Energy* **28**, 287–295.
- Bell, G., Glasstone, S., 1970. *Nuclear reactor theory*. Van Nostrand Reinhold, New York.
- Bosio, P., Burns, T.D., Ravetto, P., Rydin, R., 2001. Decoupling of neutron and delayed-neutron precursor evolutions in source-driven subcritical systems. *Kern-technik* **66**, 260–266.
- Cao, Y., Gohar, Y., Zhong, Z., 2013. Numerical studies of the flux-to-current ratio method in the kipt neutron source facility, in: *Proceedings of the International Conference on Mathematics and Computational Methods Applied to Nuclear Science and Engineering, M&C 2013*, Sun Valley, ID.
- Chartrand, R., 2011. Numerical differentiation of noisy, nonsmooth data. *ISRN Applied Mathematics* **2011**, doi:10.5402/2011/164564.
- Dulla, S., Hoh, S.S., Nervo, M., Ravetto, P., 2015a. Importance weighting of local flux measurements to improve reactivity predictions in nuclear systems. *Kern-technik* **80**, 201–207.
- Dulla, S., Nervo, M., Ravetto, P., 2014a. A method for on-line reactivity monitoring in nuclear reactors. *Annals of Nuclear Energy* **65**, 433 – 440.
- Dulla, S., Nervo, M., Ravetto, P., 2015b. Validation of the MA $\rho$ TA reactivity monitoring technique using a boiling water reactor turbine trip benchmark. *Transactions of the American Nuclear Society* **112**, 769–772.
- Dulla, S., Nervo, M., Ravetto, P., 2016. A method for the continuous monitoring of reactivity in subcritical source-driven systems. *Annals of Nuclear Energy* **87**, 1 – 11.



- Dulla, S., Nervo, M., Ravetto, P., Mila, G., Argiró, S., Beolé, S., Masera, M., Bianchini, G., Carta, M., Fabrizio, V., Peluso, V., Gabrielli, F., Rineiski, A., Kochetkov, A., Baeten, P., Uyttenhove, W., Vittiglio, G., Wagemans, J., 2014b. Interpretation of experimental measurements on the SC-1 configuration of the VENUS-F core, in: *Proceedings of the International Conference PHYSOR 2014*, Kyoto, Japan.
- Eriksson, M., Cahalan, J.E., Yang, W.S., 2005. On the performance of point kinetics for the analysis of accelerator-driven systems. *Nuclear Science and Engineering* **149**, 298–311.
- Kuramoto, R., dos Santos, A., Jerez, R., Diniz, R., 2007. Absolute measurement of  $\beta_{eff}$  based on feynman- $\alpha$  experiments and the two-region model in the IPEN/MB-01 research reactor. *Annals of Nuclear Energy* **34**, 433–442.
- Pyeon, C.H., 2014. personal communication .
- Pyeon, C.H., Hirano, Y., Misawa, T., Unesaki, H., Ichihara, C., Iwasaki, T., Shiroya, S., 2007. Preliminary Experiments on Accelerator Driven Subcritical Reactor with Pulsed Neutron Generator in Kyoto University Critical Assembly. *Journal of Nuclear Science and Technology* **44**, 1368.
- Pyeon, C.H., Nakano, H., Yamanaka, M., Yagi, T., Misawa, T., 2015. Neutron Characteristics of Solid Targets in Accelerator-Driven System with 100 MeV Protons at Kyoto University Critical Assembly. *Nuclear Technology* **192**, 181–190.
- Savitzky, A., Golay, J.E., 1964. Smoothing and differentiation of data by simplified least squares procedures. *Analytical Chemistry* **36**, 1627 – 1639.
- Shiroya, S., Unesaki, H., Kawase, Y., Moriyama, H., Inoue, M., 2000. Accelerator Driven Subcritical System as a Future Neutron Source in Kyoto University Research Reactor Institute (KURRI) - Basic Study on Neutron Multiplication in the Accelerator Driven Subcritical Reactor. *Progress in Nuclear Energy* **37**, 357.
- Shiroya, S., Yamamoto, A., Shin, K., Ikeda, T., Nakano, S., Unesaki, H., 2002. Basic Study on Accelerator Driven Subcritical Reactor in Kyoto University Research Reactor Institute (KURRI). *Progress in Nuclear Energy* **40**, 489–496.

Sjöstrand, N.G., 1956. Measurements on a subcritical reactor using a pulsed neutron source. *Archiv för Fysik* **11**, 233 – 246.